Experimental Analysis via Thermochromic Liquid Crystals of the Temperature Local Distribution in Membrane Distillation Modules

Alessandro Tamburini[a], Giorgio Micale[a], Michele Ciofalo[b], Andrea Cipollina[a,*]

[a]Dipartimento di Ingegneria Chimica, Gestionale, Informatica, Meccanica - Università degli Studi di Palermo, Viale delle Scienze Edificio 6 - 90128 Palermo ,Italy
[b] Dipartimento dell' Energia, Ingegneria dell'Informazione e Modelli Matematici - Università di Palermo, Viale delle Scienze Ed. 6, 90128 Palermo, Italy
andrea.cipollina@unipa.it

A reliable and optimized design of channels for Membrane Distillation (MD) requires knowledge of local temperature distributions within the module. This information is essential to measure the temperature polarization, choice the module configuration (net spacer features, channel size, etc) providing the best process performance. Notwithstanding such crucial aspects, only few studies have been devoted to the experimental characterization of MD channels and none of them includes data on the local temperature distribution. In the present work, an experimental technique based on the use of Thermochromic Liquid Crystals (TLCs) and digital image processing, previously proposed by the authors (Pitò et al., 2011), was further developed and employed in order to measure the temperature and local heat transfer coefficient distribution on the membrane surface in a MD spacer-filled channel. The performance of different types of commercial net spacers was tested. The channel provided with the symmetric net spacer was found to be the configuration leading to the best heat transfer and to the lowest temperature polarization.

1. Introduction

In the last four decades desalination industry has grown at a dramatically fast rate thanks to a number of different technologies (Cipollina et al., 2011a). Membrane Distillation (MD) is a recent desalination technique (Porrazzo et al., 2013) combining the features of thermal and membrane-based distillation processes (Cipollina et al., 2012;). Thermal energy supplied to saline water causes the liquid evaporation within an evaporator channel (hot channel, or feed), while a hydrophobic microporous membrane allows the passage of vapour only to a condenser channel (cold channel, or permeate), where it condenses and is collected as distillate (Figure1a).

Spacers are commonly adopted in order to promote mixing and turbulence and minimize the thickness of temperature boundary layers. Those typically employed in MD are in the form of a net, as shown in Figure1b, consisting of two overlapped layers of roughly cylindrical filaments and characterized by filament diameter df (establishing the channel thickness), hydrodynamic angles (angle θ between the filaments belonging to the two layers and angle ϕ formed with the main flow direction), voidage, or porosity, ε (free to total volume ratio) and mesh pitch lm (distance between consecutive filaments in each layer). In particular, the hydrodynamic angles control the flow pattern and represent the spacer's most important feature (Da Costa and Fane, 1994).

The presence of the spacer within a channel results in an increase of mass transfer thanks to a rise of the temperature polarization coefficient TPC (ratio between trans-membrane temperature difference T_{fm}-T_{pm} and bulk temperature difference T_{fb}-T_{pb}), which is a measure of the efficiency of heat transfer from the bulk solution to the membrane-solution interface (Yun et al., 2011).

Up to now, all studies have focused on the average values of temperature and heat flux. Little attention has been devoted to the local characterization of the spacer's influence on the separation process, despite

the fact that data on temperature distributions would allow a better understanding of temperature polarization phenomena as related to the spacer's geometry, thus guiding the choice of the most effective spacer-channel configuration. CFD studies have been presented in the literature aiming at predicting the fluid flow behaviour (Tamburini et al., 2012) and, in few cases, at locally characterizing the temperature field within spacer filled channels (Al-Sharif et al., 2013; Cipollina et al., 2009), but no validation of the predictions has been presented so far (Cipollina et al. 2011b).

The present work addresses this issue by an experimental technique based on the use of Thermochromic Liquid Crystals (TLCs) and digital image processing to measure temperature and heat transfer coefficient distributions. TLCs are commonly adopted to measure temperature distributions on a surface (TLC sheet) or in the fluid bulk (TLC droplets) (Stasiek et al., 1996; Ciofalo et al., 2000). Image analysis is a cheap way to get information (Tamburini et al., 2009) which can be employed as a valuable benchmark for CFD model validation (Tamburini et al., 2013).
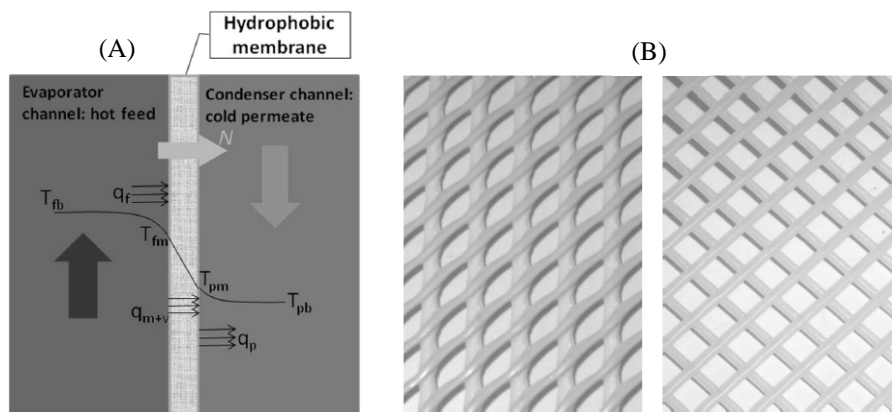

Figure 1: Principle of Membrane Distillation (left) and a typical spacer TENAX CN-11® (right)

2. Methods

The test section consists of two channels which simulate the evaporator and condenser sides of a Direct Contact MD module and are separated by a transparent polycarbonate sheet, 1 mm thick, simulating the presence of the interposed selective membrane (Figure2).
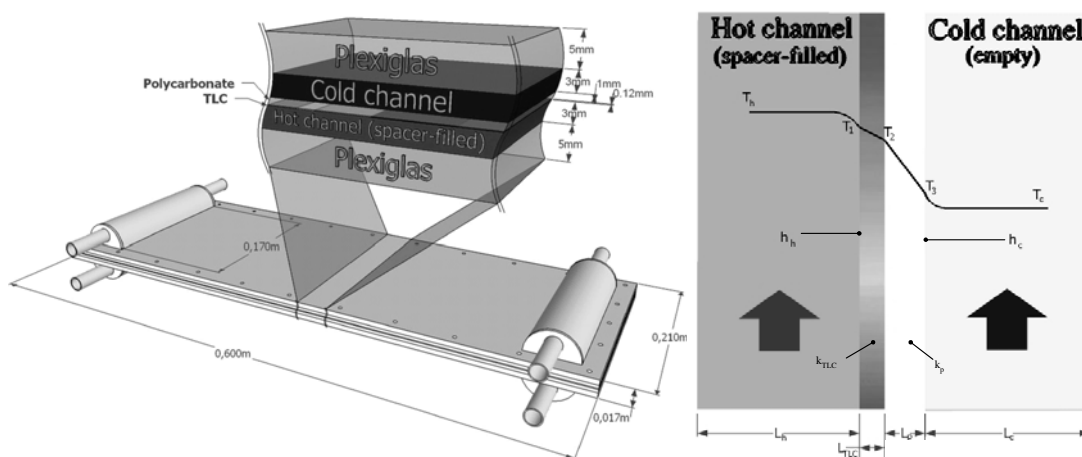

Figure 2: Sketch of the test module (left) and of the relevant temperature profile (right).

The outer walls of the channels are 10 mm thick Plexiglas® plates. The hot channel is provided with a net spacer, while the cold channel is empty (spacerless).

A TLC sheet (Hallcrest® R30C5W) is glued on the hot side of the transparent polycarbonate layer with the visible surface adhering to the wall, thus allowing photographs to be taken by a camera placed on the side of the cold channel. Each photograph provides a visualization of the instantaneous temperature field on the hot fluid/polycarbonate sheet interface. For each spacer configuration, the hot-side flow rate was made to vary from 40 L/h to 500 L/h. The corresponding Reynolds number range was that typical of real MD modules, i.e. ~200-2000 (based on the hydraulic diameter of the empty channel). In spacer-filled channels this range corresponds to transitional and low-Reynolds number turbulent flows.

All the images collected were processed by using the Matlab® Image Processing Toolbox®. They were first converted from RGB (red, green, blue) to HSL (hue, saturation, lightness) components. The use of the HSL space is preferred because it is the H (hue) component of the image that can be linked to the corresponding TLC temperature in a univocal way. The relationship between hue and temperature, i.e. the function T(H), is provided by a calibration of the TLCs, performed in situ by the steady-state method of uniform surface temperature (Abdullah et al., 2010).

With reference to the temperature profiles sketched in Figure2 (right), once the temperature T1 is determined by converting the visible TLC hue, the hot-side heat transfer coefficient h_h can be computed by assuming one-dimensional heat transfer:

$$h_h = \frac{T_1 - T_C}{(T_h - T_1)\left(\dfrac{L_{TLC}}{k_{TLC}} + \dfrac{L_P}{k_P} + \dfrac{1}{h_C}\right)} \tag{1}$$

The cold-side coefficient hc was computed by the Dittus-Boelter heat transfer correlation on the basis of the cold channel thickness and cold fluid flow rate. Distributions of local temperature and heat transfer coefficient over the hot side of the dividing membrane were thus obtained for a number of spacer configurations.

Also average heat transfer coefficients and friction coefficients were calculated for each of the configurations and flow rates investigated.

The tests regarded the two spacers in Figure1b, whose features are listed in Tab. 1.

Table 1: Geometric features of the spacers tested

Spacer	h_{sp} [mm]	θ	d_{f1} [mm]	d_{f2} [mm]	l_{m1} [mm]	l_{m2} [mm]	ε	d_h [mm]
TENAX-A	3	45°	2	1	5.2	4.4	0.63	1.53
DIAMOND	3.5	85°	2.2	2	7.4	7.5	0.73	2.72

h_{sp} [mm] = height of the channel; θ [°] = angle between crossing filaments; d_f [mm] = filament diameter; l_m [mm] = filament pitch; ε = voidage (porosity), d_h [mm] = hydraulic diameter.

Three different orientations of the Diamond spacer were tested. In Diamond-A, filaments were inclined at ±45° with respect to the main flow direction; in Diamond-B the filaments touching the TLC sheet were orthogonal to the flow while the opposite ones were roughly parallel to the same direction; finally, in Diamond-C the filaments touching the TLC sheet were parallel to the flow and the opposite ones were roughly perpendicular to it (Figure 3).
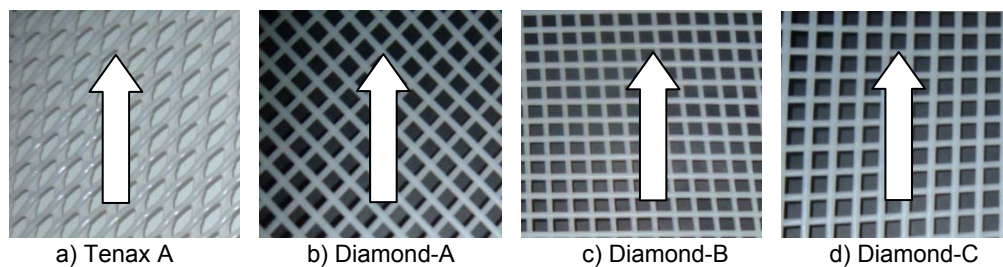

a) Tenax A   b) Diamond-A   c) Diamond-B   d) Diamond-C

Figure 3: Net spacers configurations tested

3. Results and discussion

3.1 Temperature and heat transfer coefficient distributions

During the experiments a number of images were collected and processed to obtain hue distributions. These were successively transformed (i) in corresponding temperature distributions by the H-T calibration curve, and (ii) in corresponding heat transfer coefficient distributions by Eq. 1. As an example, Figure 4 shows typical results, including original snapshot (Figure4a) and the corresponding hue distribution (Figure 4b) for the case of the Diamond-B orientation. The H distributions relevant to images collected by investigating different zones of the domain (where the fluid flow is "periodic fully developed") were averaged. Figure4c and Figure4d report the corresponding temperature and heat transfer coefficient distributions, respectively.

With reference to Figure4d, and regardless of the actual spatial orientation of the filaments, the least heat transfer coefficients (h_h<1000 W/m^2 K) occur in the areas where the filaments touch the TLC sheet. Immediately downstream of these areas, regions with intermediate heat transfer rates (1000<h_h<2000 W/m^2 K) are found: these presumably coincide with the recirculation bubbles where the fluid vein remains detached. Finally, zones of high heat transfer (h_h>2000 W/m^2 K) can be observed immediately upstream of the next filament; they presumably coincide with the regions where the fluid vein reattaches on the wall and intense mixing occurs. Thus, zones of mixing and calm periodically alternate according to the spacer pitch and to the orientation of its filaments.
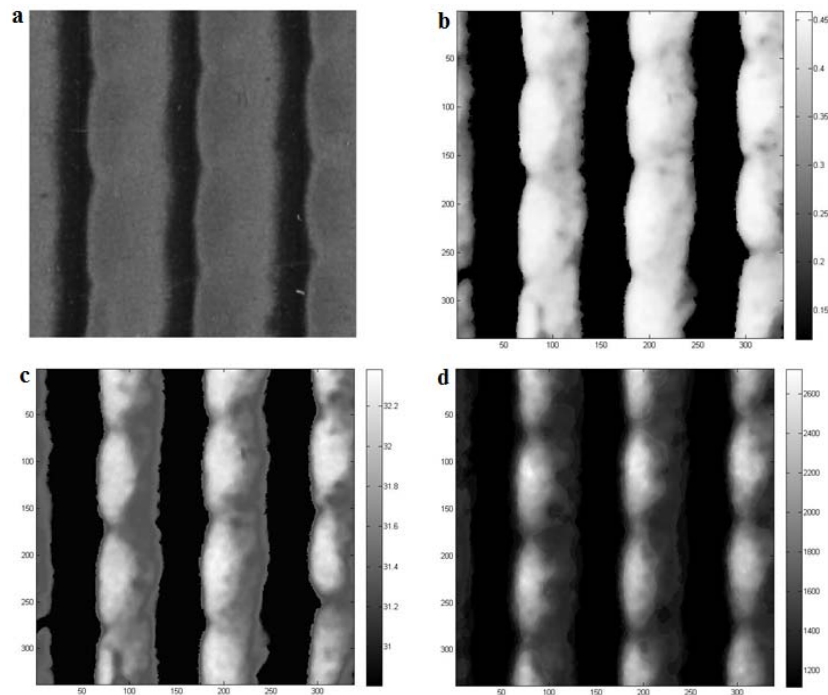

Figure 4: Diamond-B configuration maps (flow from right to left). a) Typical region of interest showing the TLC surface; b) False-colour map of hue H; c) False-colour map of the local temperature T [°C]; d) False-colour map of h_h [W/m^2 K].

3.2 Assessment of the effect of spacer orientation in a MD module

As mentioned above, three spatial orientations of the same Diamond spacer were tested with the aim to assess the effect of the filaments orientation on heat transport and to identify the best configuration in terms of reduction of temperature polarization. For each spacer orientation, surface-averaged heat transfer coefficients were measured as functions of the hot water flow rate. All the experimental results collected were made dimensionless in the form of Nusselt number Nu and were reported as functions of the Reynolds number Re (Figure 5). Nu and Re were calculated on the basis of the mean fluid velocity and of the channel height.

Nu exhibits a low but clear dependence on Re (exponents ranging from ~0.14 to ~0.27). A Nusselt number equal to 5.38 was computed analytically for laminar flow in a corresponding empty channel by solving the heat transport equations under the assumptions of Hagen-Poiseuille fluid flow between two indefinite flat plates, one with constant heat flux and the other adiabatic. All the spacer-filled channels tested including those investigated in previous work by the same research group (Pitò et al., 2011) provided Nusselt numbers higher than this value, thus confirming that spacers enhance heat transport by promoting fluid mixing and reducing polarization effects.
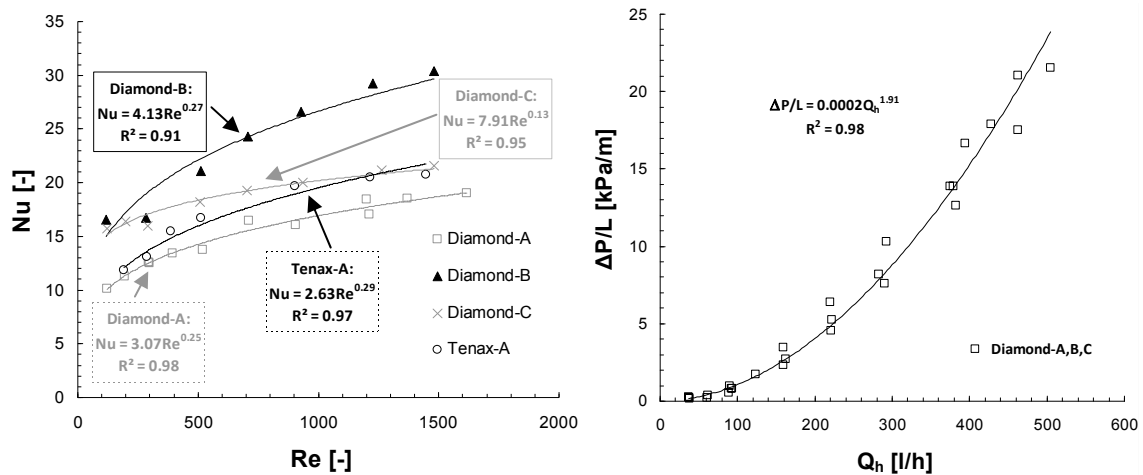

Figure 5: Left: Nusselt number vs Reynolds number; right: pressure vs hot fluid flow rate (Tenax-A data not available).

Figure5 shows that the Diamond-B orientation is the one which exhibits the highest values of Nu. Thus, the presence of filaments orthogonal to the flow in the proximity of the active wall (i.e., that where heat transfer is measured) seems to best promote heat transfer by providing high-mixing reattachment regions, in which turbulent flow presumably occurs. Note that similar separation and reattachment phenomena occur also with the Diamond-A orientation, but they take place on the wall opposite to that where the heat transfer measurements are taken.

These findings are in agreement with those by Da Costa and Fane (1994), who investigated the impact of spacer orientation on mass transfer in flat channels for ultra-filtration. According to their study, two-layer spacers with the filaments of one layer parallel to the main flow direction, and thus inducing no directional flow change, and the filaments of the other layer (placed next to the membrane) orthogonal to the flow, perform better than spacers with the same voidage arranged symmetrically at 45° with respect to the flow, and thus inducing criss-cross flow paths.

The left graph in Figure5 shows also the results relevant to the asymmetric spacer Tenax A. Nu values were found to be always lower than those provided by the Diamond-B orientation. In particular, Nu data obtained with the Tenax A spacer appear similar to those provided by the Diamond-A orientation at low Re and similar to those provided by the Diamond-C orientation at high Re.

In the present work also the pressure drop induced by the presence of the spacer was measured for each of the three Diamond orientations. Very similar pressure drops were found for the three orientations, so that the relevant results are reported with the same symbol in Figure 5 (right). The dependence of the pressure drop on the mean fluid velocity was found to be almost-quadratic, in agreement with the assumption of turbulent flow.

According to the present results, it is worth noting that the Reynolds analogy (which predicts a proportionality between the Stanton number and the friction coefficient) is not valid for the present system. In fact, Nu increases as a weak power of Re, with an exponent ranging from 0.13 (Diamond-C) to 0.27 (Diamond-B) and 0.29 (Tenax-A), so that $St=Nu/(Re\ Pr)$ varies as a power of Re with an exponent ranging from -0.87 to -0.73 (-0.71 for Tenax-A). On the other hand, as Figure5 (right) shows, the friction coefficient varies as a power of Re with an exponent of about -0.1. This indicates that the drag induced by the spacer is mostly related to inertial effects (repeated expansions and contractions of the available cross section) rather than skin friction-related.

4. Conclusions

A thermographic technique based on thermochromic liquid crystals (TLCs), presented in a previous work (Pitò et al., 2011) was further developed in order to investigate heat transfer and temperature polarization in spacer-filled channels for Membrane Distillation modules.

Three different orientations of a net spacer made of two layers of almost-perpendicular overlapped filaments (Diamond) were investigated; also an asymmetric spacer (Tenax-A) was tested for comparison purposes. Experimental results can be summarized as follows:

•Independently of the orientation of the spacer wires in contact with the TLC sheet, the heat transfer coefficient reaches (i) low values in the "dead" regions where the spacer filaments touch the wall, (ii) intermediate values downstream of these contact areas, presumably in correspondence with separated flow regions, and (iii) highest values immediately upstream of the subsequent filaments, presumably in correspondence with reattachment regions where the velocity component perpendicular to the conductive wall is significant.

•In all the geometries tested, the increase of the Nusselt number with the Reynolds number follows a weak power law. All the Nusselt number values obtained for the spacer-filled channels were from 2 up to 5.5 times larger than that calculated for the case of a corresponding empty (spacerless) channel.

•Among the Diamond orientations tested, Diamond-B was found to be the most effective in reducing temperature polarization, followed by Diamond-C and finally by Diamond-A. The same order of efficiency was found by Da Costa and Fane (1994) for the case of spacer-filled channels devoted to ultra filtration processes.

•An almost-quadratic dependence of pressure drops on the mean fluid velocity was found, suggesting that the spacer-induced drag is related to inertial effects rather than to skin-friction effects.

References

Abdullah N., Abu Talib A.R., Jaafar A.A., Salleh M.A.M., 2010, The basics and issues of Thermochromic Liquid Crystal Calibration, Experimental Thermal and Fluid Science, 34, 1089-1121.

Al-Sharif S., Albeirutty M., Cipollina A., Micale G., 2013, Modelling flow and heat transfer in spacer-filled membrane distillation channels using open source CFD code, Desalination, 311, 103-112.

Ciofalo M., Di Piazza I., Stasiek J. A., 2000, Investigation of flow and heat transfer in corrugated-undulated plate heat exchangers, Heat and Mass Transfer, 36, 449-462.

Cipollina A., Di Miceli A., Koschikowski J., Micale G., Rizzuti L., 2009, CFD simulation of a membrane distillation module channel, Desalination and Water Treatment, 6, 177-183.

Cipollina A., Di Sparti M.G., Tamburini A., Micale G., 2012, Development of a Membrane Distillation module for solar energy seawater desalination, Chemical Engineering Research and Design, 90, 2101-2121.

Cipollina A., Micale G., Noto S., Brucato A., 2011a, Multi stage flash desalination with direct mixing condensation, Chemical Engineering Transactions, 24, 1555-1560, DOI: 10.3303/CET1124260

Cipollina A., Micale G., Rizzuti L., 2011b, Membrane distillation heat transfer enhancement by CFD analysis of internal module geometry. Desalination and Water Treatment. 25, 195-209.

Da Costa A.R., Fane A.G., 1994, Net-type spacers: effect of configuration on fluid flow path and ultrafiltration flux. Industrial Engineeering Chemistry Research, 33, 1845-1851.

Pitò P., Cipollina A., Micale G., Ciofalo M., 2011, Characterization of spacer-filled membrane distillation modules by thermochromic liquid crystals, XXIX UIT Heat Transfer Conference, Turin, Italy .

Porrazzo R., Cipollina A., Galluzzo M., Micale G., 2013, A neural network-based optimizing control system for a seawater-desalination solar-powered membrane distillation unit, Comp. Chem. Eng., 54, 79-96.

Stasiek J.A., Colliins M. W., Ciofalo M., Chew P.E., 1996, Investigation of flow and heat transfer in corrugated passages – I. Experimental results, Int. J. Heat Mass Transfer, 39, 149-164.

Tamburini A., Cipollina A., Micale G., Brucato A., 2013, Particle distribution in dilute solid liquid unbaffled tanks via a novel laser sheet and image analysis based technique, Chem. Eng. Sci., 87, 341-358.

Tamburini A., La Barbera G., Cipollina A., Ciofalo M., Micale G., 2012, CFD simulation of channels for direct and reverse electrodialysis, Desalination and Water Treatment, 48, 370–389.

Tamburini, A., Gentile, L., Cipollina, A., Micale, G., Brucato, A., 2009. Experimental investigation of dilute solid-liquid suspension in an unbaffled stirred vessels by a novel pulsed laser based image analysis technique, Chemical Engineering Transactions, 17, 531-536.

Yun Y., Wang J., Ma R., Fane A.G., Effects of channel spacers on direct contact membrane distillation, Des. & Water Treatment 34, 2011, pp. 63-69.